Sensorless Synchronous Reluctance Generator Control Based on q Axis Estimated Current

Liviu – Dănuț Vitan
Department of Electrical Engineering
Politehnica University of Timisoara
Timisoara, Romania
liviu.vitan@student.upt.ro

Lucian Tutelea
Department of Electrical Engineering
Politehnica University of Timisoara
Timisoara, Romania
lucian.tutelea@upt.ro

Nicolae Muntean
Department of Electrical Engineering
Politehnica University of Timisoara
Romanian Academy, Timisoara Branch
Timisoara, Romania
nicolae.muntean@upt.ro

Ion Boldea
Department of Electrical Engineering
Politehnica University of Timisoara
Romanian Academy, Timisoara Branch
Timisoara, Romania
ion.boldea@upt.ro

***Abstract*—This paper presents a sensorless Synchronous Reluctance Machine used as a generator with a different method for rotor position estimator. The estimator is based on the machine model and the error between measured q-axis current versus estimated current. The rotor position error is analyzed in various running conditions considering uncertain machine parameters. Stability of the rotor position estimator has been approached using model linearization by small signal deviations. Simulation and experimental results validate the theoretical assumptions.**

Keywords—Synchronous reluctance machine, rotor position estimator, rotor position sensitivity, stability, sensorless control.

I. INTRODUCTION

The Synchronous Reluctance Machine (SynRM) has gained researchers attention in the last period due to its advantages as a simple and rugged structure, no rotor winding and no PMs [1]–[5]. Over the years, substantial research on SynRM design [2], [6]–[9], directly conected to the grid [10]–[12], and inverter fed with position sensor control [13]–[16] has been done. Also, sensorless methods regarding rotor position has been approached in [17]–[22]. For small power and low speed applications, sensorless control is essential to have a low-cost implementation. State-of-the-art estimators are based on measured voltages integration, usually implemented as low pass filters that introduce distortions at low speed, or on signal injection [23] which needs a DC voltage reserve.

This paper proposes a rotor position estimator for a SynRM based on machine model and q-axis current error (measured and estimated by model). In this method, the integration operations for the flux observer are naturally included in the closed loop of the machine model thus additional loops for offset and fluxes initial values compensation are not required. Also, the aperiodic flux component damping from the observer is similar with the electrical machine phenomena. An existing SynRM was controlled in generator mode with dq current references in order to verify the study.

II. SYSTEM LAYOUT

The proposed configuration of sensorless control used for controlling the Synchronous Reluctance Generator (SynRG) is shown in Fig.1. It consists of a Prime Mover, a SynRG and a power converter which delivers the energy in a DC grid.

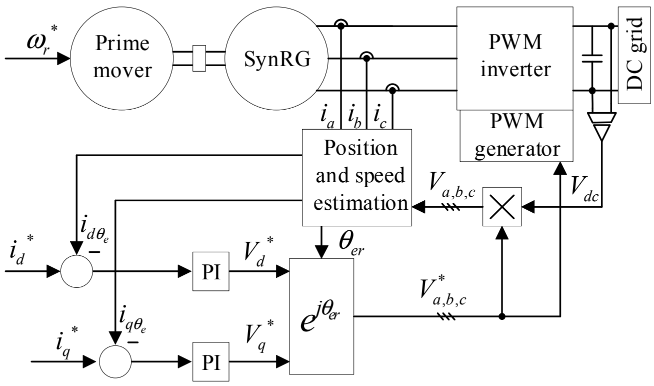

Fig. 1. Sensorless control diagram of SynRG

The Prime Mover can be a hydro turbine, a wind turbine or a variable speed drive (VSD) with speed control. The power reference of the SynRG is obtained by prescribing the d- and q-axes currents. The current errors are processed through a PI controller in order to produce the dq reference voltages. The dq reference voltages are transformed into polar coordinates to be prescribed to the PWM inverter. In order to calculate the rotor frame coordinates, the angular position is needed and it is estimated by measuring the phase currents and DC voltage.

A. SynRG Model

The SynRG is characterized by the following equations in rotating frame reference:

$$\frac{d\psi_d}{dt} = V_d - i_d \cdot R_s + p_1 \cdot \omega_r \cdot \psi_q, \tag{1}$$

$$\frac{d\psi_q}{dt} = V_q - i_q \cdot R_s - p_1 \cdot \omega_r \cdot \psi_d, \tag{2}$$

$$\frac{d\omega_r}{dt} = \frac{1}{J}\left(T_{em} - T_L\right), \tag{3}$$

$$\frac{d\theta_r}{dt} = \omega_r, \quad T_{em} = p_1\left(\psi_d \cdot i_q - \psi_q \cdot i_d\right), \tag{4}$$

$$\psi_d = L_d \cdot i_d, \quad \psi_q = L_q \cdot i_q. \tag{5}$$

where ψ_d, ψ_q are the d- and q-axis linkage flux, V_d, V_q are the d- and q-axis voltages, R_s is the stator resistance, i_d, i_q are the d- and q-axis currents, p_1 is the number of pole pairs, L_d, L_q are the d- and q-axis inductances, ω_r is the rotor speed, θ_r is the rotor position, T_{em} is the electromagnetic torque, T_L is load torque and J is the entire system (prime mover and SynRG) inertia.

B. Rotor position-speed estimator

The overall performances of the system depends on the rotor position estimation, which is based on the same model as the machine, except for the mechanical equation which is replaced with a PI transfer function acting on the estimated and the machine q axis currents (with the machine q axis current in the estimated dq frame). Also for estimation of torque, the active flux concept is used [24]. Fig. 2 shows the implementation of position-speed estimator. The equations which describe the estimator subsystem are given below:

$$\frac{d\psi_{de}}{dt} = V_{d\theta_e} - i_{de}\cdot R_{se} + p_1\cdot\omega_{re}\cdot\psi_{qe}, \tag{6}$$

$$\frac{d\psi_{qe}}{dt} = V_{q\theta_e} - i_{qe}\cdot R_{se} - p_1\cdot\omega_{re}\cdot\psi_{de}, \tag{7}$$

$$\frac{d\omega_{re}}{dt} = k_p\cdot\frac{d\varepsilon_{\omega re}}{dt} + k_i\cdot\varepsilon_{\omega re}, \tag{8}$$

$$\frac{d\theta_{re}}{dt} = \omega_{re}, \tag{9}$$

$$T_{em_e} = \left(\psi_{de} - i_{d\theta_e}\cdot L_{qe}\right)\cdot p_1\cdot i_{q\theta_e}, \tag{10}$$

$$i_{de} = \frac{\psi_{de}}{L_{de}},\quad i_{qe} = \frac{\psi_{qe}}{L_{qe}},\quad \varepsilon_{\omega re} = i_{qe} - i_{q\theta_e}. \tag{11}$$

where the terms with index 'e' are the estimated values and they have the same signification as in SynRG model. The terms: $V_{d\theta_e}$, $V_{q\theta_e}$, $i_{d\theta_e}$, $i_{q\theta_e}$ are d- and q-axis voltages and currents in estimator coordinates (these were obtained from stator coordinates through inverse Park transform using estimated rotor position), k_p, k_i are the PI transfer function constants, $\varepsilon_{\omega re}$ is the error between estimated and measured q-axis currents.

III. POSITION ERORR ANALYSIS REGARDING PARAMETERS VARIATION

The estimated angle error, versus uncertain machine parameters is analyzed in this chapter. The machine and estimator subsystems both use the same phase voltages that are provided from V_d^*, V_q^*, in the estimated dq reference frame. This differs from the machine dq frame with error angle ε_θ.

$$V_d = V_d^*\cdot\cos(\varepsilon_\theta) + V_q^*\cdot\sin(\varepsilon_\theta) \tag{12}$$

$$V_q = -V_d^*\cdot\sin(\varepsilon_\theta) + V_q^*\cdot\cos(\varepsilon_\theta) \tag{13}$$

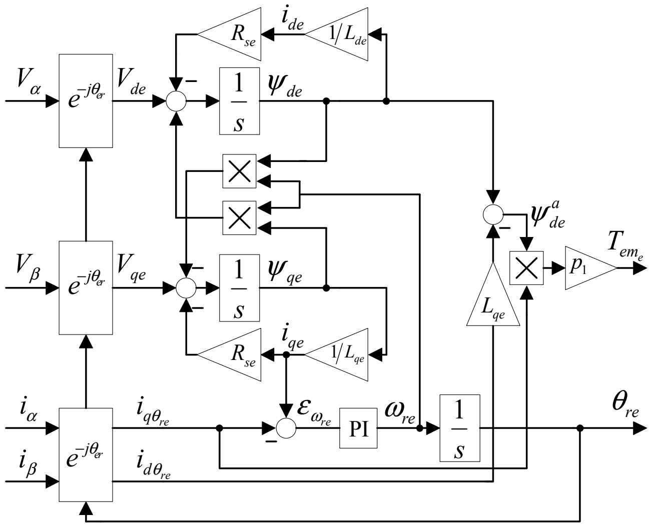

Fig. 2. Block diagram of the Position Estimator

$$i_{d\theta e} = \frac{\psi_d}{L_d}\cdot\cos(\varepsilon_\theta) - \frac{\psi_q}{L_q}\cdot\sin(\varepsilon_\theta) \tag{14}$$

$$i_{q\theta e} = \frac{\psi_q}{L_q}\cdot\cos(\varepsilon_\theta) + \frac{\psi_d}{L_d}\cdot\sin(\varepsilon_\theta) \tag{15}$$

$$\varepsilon_\theta = p_1(\theta_r - \theta_{re}) \tag{16}$$

Taking into consideration the machine voltages (12) and (13), the machine currents in the estimator reference (14) and (15), the machine equations and estimator equations, the entire system (machine and estimator) equations becomes:

$$\frac{d\psi_d}{dt} = V_d^*\cdot\cos(\varepsilon_\theta) + V_q^*\cdot\sin(\varepsilon_\theta) - \frac{R_s}{L_d}\cdot\psi_d + \\ + p_1\cdot\omega_r\cdot\psi_q, \tag{17}$$

$$\frac{d\psi_q}{dt} = -V_d^*\cdot\sin(\varepsilon_\theta) + V_q^*\cdot\cos(\varepsilon_\theta) - \frac{R_s}{L_q}\cdot\psi_q \\ - p_1\cdot\omega_r\cdot\psi_d, \tag{18}$$

$$\frac{d\omega_r}{dt} = \frac{1}{J}\left[p_1\cdot\psi_d\cdot\psi_q\left(\frac{1}{L_q} - \frac{1}{L_d}\right) - T_L\right], \tag{19}$$

$$\frac{d\theta_r}{dt} = \omega_r,\quad \frac{d\theta_{re}}{dt} = \omega_{re}, \tag{20}$$

$$\frac{d\psi_{de}}{dt} = V_d^* - \frac{R_{se}}{L_{de}}\cdot\psi_{de} + p_1\cdot\omega_{re}\cdot\psi_{qe}, \tag{21}$$

$$\frac{d\psi_{qe}}{dt} = V_q^* - \frac{R_{se}}{L_{qe}}\cdot\psi_{qe} - p_1\cdot\omega_{re}\cdot\psi_{de}, \tag{22}$$

$$\frac{d\omega_{re}}{dt} = k_p\cdot\frac{d}{dt}\left(\frac{\psi_{qe}}{L_{qe}} - \frac{\psi_q}{L_q}\cdot\cos(\varepsilon_\theta) - \frac{\psi_d}{L_d}\cdot\sin(\varepsilon_\theta)\right) \\ + k_i\cdot\frac{\psi_{qe}}{L_{qe}} - \left(\frac{\psi_q}{L_q}\cdot\cos(\varepsilon_\theta) + \frac{\psi_d}{L_d}\cdot\sin(\varepsilon_\theta)\right), \tag{23}$$

A steady state solution of the system equations (17)-(23), result in constant state variables, so their derivatives are zero, except for (20) in this case. Solving the system equations, the following results are obtained:

$$\psi_{de} = \frac{L_{de} \cdot \left(R_{se} \cdot V_d^* + p_1 \cdot \omega_r \cdot L_{qe} \cdot V_q^* \right)}{\Delta_e}, \tag{24}$$

$$\psi_{qe} = \frac{L_{qe} \cdot \left(R_{se} \cdot V_q^* - p_1 \cdot \omega_r \cdot L_{de} \cdot V_d^* \right)}{\Delta_e}, \tag{25}$$

$$\begin{aligned} \psi_d = \frac{L_d}{\Delta} \cdot \Big[& R_s \cdot \left(V_d^* \cdot \cos(\varepsilon_\theta) + V_q^* \cdot \sin(\varepsilon_\theta) \right) + \\ & + X_q \cdot \left(-V_d^* \cdot \sin(\varepsilon_\theta) + V_q^* \cdot \cos(\varepsilon_\theta) \right) \Big], \end{aligned} \tag{26}$$

$$\begin{aligned} \psi_q = \frac{L_q}{\Delta} \cdot \Big[& R_s \cdot \left(-V_d^* \cdot \sin(\varepsilon_\theta) + V_q^* \cdot \cos(\varepsilon_\theta) \right) - \\ & - X_d \cdot \left(V_d^* \cdot \cos(\varepsilon_\theta) + V_q^* \cdot \sin(\varepsilon_\theta) \right) \Big]. \end{aligned} \tag{27}$$

where:

$$\begin{aligned} & \Delta_e = R_{se}^2 + p_1^2 \cdot \omega_r^2 \cdot L_{de} \cdot L_{qe}, \quad X_d = p_1 \cdot \omega_r \cdot L_d, \\ & \Delta = R_s^2 + L_d \cdot L_q \cdot \omega_r^2 \cdot p_1^2, \quad X_q = p_1 \cdot \omega_r \cdot L_q. \end{aligned} \tag{28}$$

from (23) result:

$$\frac{\psi_{qe}}{L_{qe}} = \left(\frac{\psi_q}{L_q} \cdot \cos(\varepsilon_\theta) + \frac{\psi_d}{L_d} \cdot \sin(\varepsilon_\theta) \right). \tag{29}$$

The equation (30) is calculated by using (24) - (27) into (29).

$$a \cdot \cos(2\varepsilon_\theta) - b \cdot \sin(2\varepsilon_\theta) + e = 0 \tag{30}$$

where:

$$\begin{cases} a' = R_{se} \cdot V_q^* - X_{de} \cdot V_d^*, \quad a = -\dfrac{V_d^*}{2} \cdot X_d + \dfrac{V_d^*}{2} \cdot X_q \\ b = \dfrac{V_q^*}{2} \cdot \left(X_d - X_q \right) \\ f = R_s \cdot V_q^* - \dfrac{V_d^*}{2} \cdot \left(X_d + X_q \right), \quad e = f - a' \cdot k_\Delta \end{cases} \tag{31}$$

Solutions:

$$\begin{cases} \varepsilon_\theta = \pi \cdot k - \tan^{-1}\left(\dfrac{b - \sqrt{a^2 + b^2 - e^2}}{a - e} \right) \\ \varepsilon_\theta = \pi \cdot k - \tan^{-1}\left(\dfrac{b + \sqrt{a^2 + b^2 - e^2}}{a - e} \right) \end{cases} \tag{32}$$

Conditions:

$$\begin{cases} e^2 \le a^2 + b^2 \\ \dfrac{b \mp \sqrt{a^2 + b^2 - e^2}}{a - e} \in \mathbb{R} \end{cases} \tag{33}$$

The per unit stator resistance k_r, d-axis inductance k_d and q-axis inductances k_q, were introduced to consider the uncertain parameters in the estimator. The estimator parameters related to machine parameters become:

$$R_{se} = k_r \cdot R_s, \quad L_{de} = k_d \cdot L_d, \quad L_{qe} = k_q \cdot L_q. \tag{34}$$

The algebraic equation system does not have real solutions for the high difference between estimator and machine parameters, which means there is no steady state regime. In Fig. 3 and Fig. 4 it is shown how ε_θ depends according to the variation of k_r, k_d and k_q (0.5 to 1.5 with 0.05 step) at several rotor speeds and different i_q/i_d ratio. The extensive simulations show that position error depends only on the i_q/i_d currents ratio, and their absolute values have no influence.

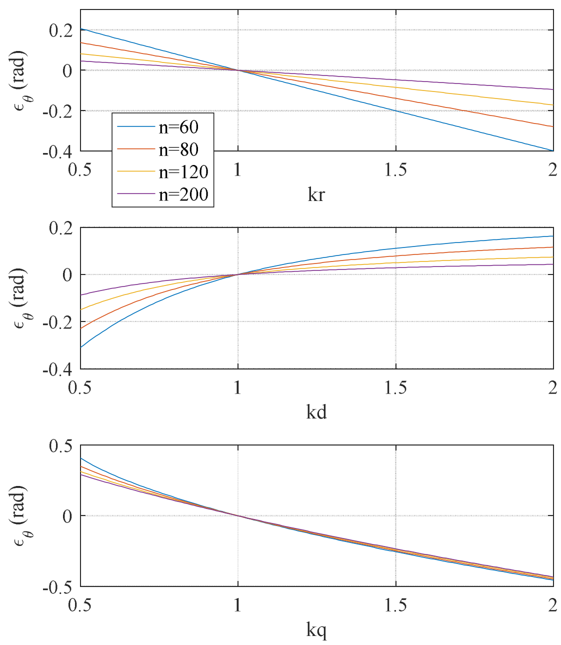

Fig. 3. Position error sensitivity at equal currents ($i_d = 5$, $i_q = -5$)

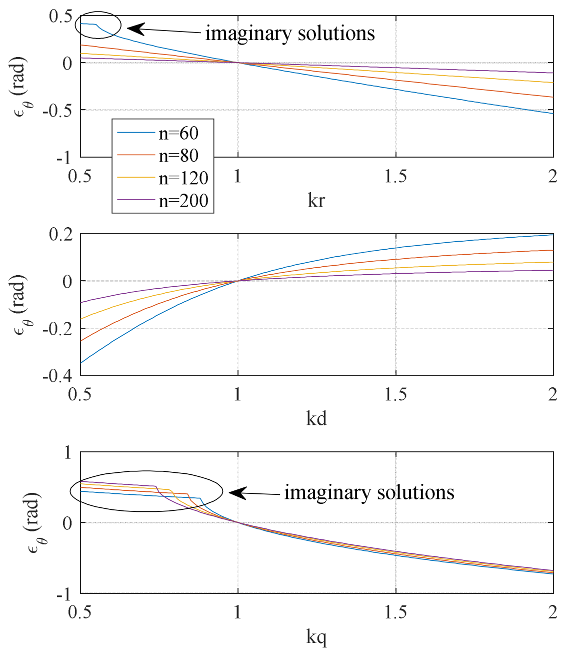

Fig. 4. Potion error sensitivity at current ratio $i_q / i_d = 2$ ($i_d = 5$, $i_q = -10$)

IV. STABILITY ANALYSIS

The steady state analysis from previous chapter shows the position error according to parameter variation, but it is not able to prove that a steady state solution is stable and how the PI transfer function constants of the estimator, k_p, k_i influence the stability, so a stability analysis is required. The analysis was performed by linearization, considering small variations in the state variables around a steady state point.

$$\psi_d = \psi_{d_0} + \tilde{\psi}_d \, , \; \psi_q = \psi_{q_0} + \tilde{\psi}_q \tag{35}$$

$$\psi_{de} = \psi_{de_0} + \tilde{\psi}_{de} \, , \; \psi_{qe} = \psi_{qe_0} + \tilde{\psi}_{qe} \tag{36}$$

$$\omega_{re} = \omega_{re_0} + \tilde{\omega}_{re} \, , \; \theta_r = \theta_{r_0} + \tilde{\theta}_r \, , \; \theta_{re} = \theta_{re_0} + \tilde{\theta}_{re} \tag{37}$$

$$\frac{d}{dt}\varepsilon_\theta = p_1 \cdot \left(\omega_r - \omega_{re}\right) \tag{38}$$

Considering system equations from (17)-(23) and equation (38) and substituting the state variables with their expressions from (35) to (37), the linearized system equation are obtained:

$$\begin{aligned} \frac{d}{dt}\tilde{\psi}_d = & -\frac{R_s}{L_d}\cdot\tilde{\psi}_d + p_1\cdot\omega_r\cdot\tilde{\psi}_q + \\ & +\tilde{\varepsilon}_\theta\cdot\left[V_q^*\cdot\cos\left(\varepsilon_{\theta_0}\right) - V_d^*\cdot\sin\left(\varepsilon_{\theta_0}\right)\right], \end{aligned} \tag{39}$$

$$\begin{aligned} \frac{d}{dt}\tilde{\psi}_q = & -p_1\cdot\omega_r\cdot\tilde{\psi}_q - \frac{R_s}{L_d}\cdot\tilde{\psi}_d - \\ & -\tilde{\varepsilon}_\theta\cdot\left[V_d^*\cdot\cos\left(\varepsilon_{\theta_0}\right) - V_q^*\cdot\sin\left(\varepsilon_{\theta_0}\right)\right], \end{aligned} \tag{40}$$

$$\frac{d}{dt}\tilde{\psi}_{de} = -\frac{R_{se}}{L_{de}}\cdot\tilde{\psi}_{de} + p_1\cdot\omega_{re_0}\cdot\tilde{\psi}_{qe} + p_1\cdot\psi_{qe_0}\cdot\tilde{\omega}_{re}, \tag{41}$$

$$\frac{d}{dt}\tilde{\psi}_{qe} = -p_1\cdot\omega_{re_0}\cdot\tilde{\psi}_{de} - \frac{R_{se}}{L_{qe}}\cdot\tilde{\psi}_{qe} - p_1\cdot\psi_{de_0}\cdot\tilde{\omega}_{re}, \tag{42}$$

$$\frac{d}{dt}\tilde{\omega}_{re} = \left(\begin{bmatrix} a_{11} & a_{12} \\ a_{21} & a_{22} \\ a_{31} & 0 \\ a_{41} & a_{42} \\ a_{51} & 0 \\ a_{61} & a_{62} \end{bmatrix}\cdot\begin{bmatrix} k_p \\ k_i \end{bmatrix}\right)^T\cdot\begin{bmatrix} \tilde{\psi}_d \\ \tilde{\psi}_q \\ \tilde{\psi}_{de} \\ \tilde{\psi}_{qe} \\ \tilde{\omega}_{re} \\ \tilde{\varepsilon}_\theta \end{bmatrix}, \tag{43}$$

where:

$$\begin{aligned} a_{11} = & \frac{R_s\cdot\sin\left(\varepsilon_{\theta_0}\right)}{L_d^{\,2}} - p_1\cdot\left(\omega_r - \omega_{re_0}\right)\cdot\frac{\cos\left(\varepsilon_{\theta_0}\right)}{L_d} + \\ & +\frac{p_1\cdot\omega_r\cdot\cos\left(\varepsilon_{\theta_0}\right)}{L_q}, \end{aligned} \tag{44}$$

$$a_{12} = -\frac{\sin\left(\varepsilon_{\theta_0}\right)}{L_d^{\,2}}, \; a_{22} = \frac{\cos\left(\varepsilon_{\theta_0}\right)}{L_q^{\,2}}, \tag{45}$$

$$\begin{aligned} a_{21} = & \frac{R_s\cdot\cos\left(\varepsilon_{\theta_0}\right)}{L_q^{\,2}} - p_1\cdot\left(\omega_r - \omega_{re_0}\right)\cdot\frac{\sin\left(\varepsilon_{\theta_0}\right)}{L_q} - \\ & -\frac{p_1\cdot\omega_r\cdot\sin\left(\varepsilon_{\theta_0}\right)}{L_d}, \end{aligned} \tag{46}$$

$$a_{31} = -\frac{p_1\cdot\omega_{re_0}}{L_{qe}}\, , \; a_{41} = -\frac{R_{se}}{L_{qe}^2}\, , \; a_{42} = \frac{1}{L_{qe}}, \tag{47}$$

$$a_{51} = p_1\cdot\frac{\psi_{d_0}\cdot\cos\left(\varepsilon_{\theta_0}\right)}{L_d} - \frac{\psi_{q_0}\cdot\sin\left(\varepsilon_{\theta_0}\right)}{L_q} - p_1\cdot\frac{\psi_{de_0}}{L_{qe}}, \tag{48}$$

$$\begin{aligned} a_{61} = & \left(\frac{1}{L_d} - \frac{1}{L_q}\right)\cdot\left\{V_d^*\cdot\cos\left(2\varepsilon_{\theta_0}\right) + V_q^*\cdot\sin\left(2\varepsilon_{\theta_0}\right) + \right. \\ & \left. +p_1\cdot\omega_r\cdot\left[\psi_{q_0}\cdot\cos\left(\varepsilon_{\theta_0}\right) - \psi_{d_0}\cdot\sin\left(\varepsilon_{\theta_0}\right)\right]\right\} - \\ & -R_s\cdot\left[\frac{\psi_{d_0}}{L_d^2}\cdot\cos\left(\varepsilon_{\theta_0}\right) + \frac{\psi_{q_0}}{L_q^2}\cdot\sin\left(\varepsilon_{\theta_0}\right)\right] + \\ & +p_1\cdot\omega_{re_0}\cdot\left[\frac{\psi_{d_0}}{L_d}\cdot\sin\left(\varepsilon_{\theta_0}\right) + \frac{\psi_{q_0}}{L_q}\cdot\cos\left(\varepsilon_{\theta_0}\right)\right], \end{aligned} \tag{49}$$

$$a_{62} = \frac{\psi_{q_0}}{L_q}\cdot\sin\left(\varepsilon_{\theta_0}\right) - \frac{\psi_{d_0}}{L_d}\cdot\cos\left(\varepsilon_{\theta_0}\right), \tag{50}$$

$$\frac{d}{dt}\tilde{\varepsilon}_\theta = -p_1\cdot\omega_{re_0}. \tag{51}$$

The Hurwitz criterion was used to study the system stability. Based on the six order equation system (39)-(43) and (51), the system transfer function was calculated considering the machine parameters (TABLE I.), several values for rotor speed (60, 120 and 200 rpm) and several id, iq combinations. Although Hurwitz minors are available in analytical form, their expressions are too complex to be analyzed and aggregated for thousands of combinations (around 90000). Again, the numerical solution should be used by giving values to k_p and k_i. To explore a large domain (1 to one million) without impractical computation effort, an exponential distribution, with only 101 values per constant, (10201 total values) is used.

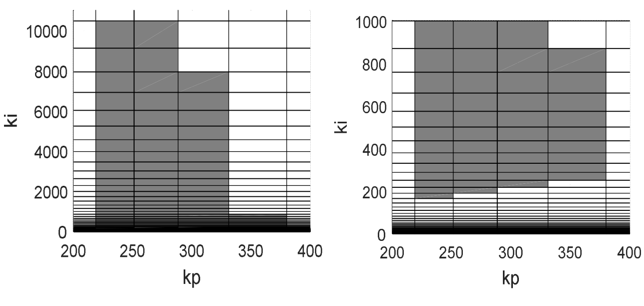

Fig. 5. Feasibility domain for k_p and k_i: all domain - left, close-up - right

TABLE I. PARAMETERS OF THE SYNRG

Parameters	***Value***	***Unit***
Rated power P_N	1800	W
Line voltage V_L	400	V
Rated current I_N	10	A
Rated speed n_N	200	rpm
Pole pairs p_1	6	
d-axis inductance L_d	0,822	H
q-axis inductance L_q	0,289	H
Stator phase resistance R_s	6,17	Ω

A feasibility matrix, containing 1 for stable points and zero for unstable was built. The final feasibility matrix was computed as a set of intersection of all feasibility matrix. The feasibility domain (matrix) for k_p and k_i is shown in Fig. 5.

V. SIMULATION RESULTS

Stability analysis studied in previous chapter needs a validation through simulation of the entire system (Fig. 1) because the simulation provides access to the machine parameters. The digital simulation is based on the diagram block presented in Fig. 1, where SynRG and Prime Mover model are shown in Fig. 9, and estimator model from Fig. 2. In Fig. 9, the prime mover is a torque controller in order to drive the SynRG.

The results of the simulation were obtained for $k_p = 250$ and $k_i = 1500$ from Fig. 5 and the parameters for SynRG from TABLE I. The following cases are presented:

- Around rated power, n=200rpm: Fig. 6, Fig. 7;
- Rated torque, n=120rpm: Fig. 8, Fig. 10.

The saturation and variation of stator resistance with temperature were considered by modifying the machine parameters.

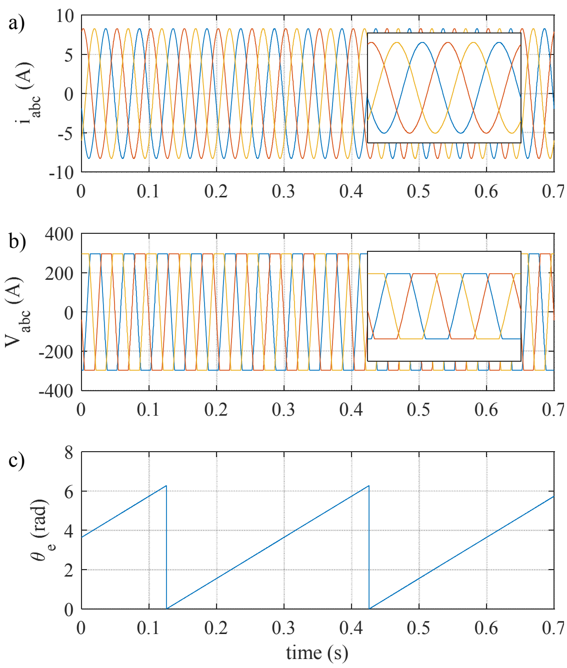

Fig. 6. High power results: i_d= 5; i_q= -10, Rs = 6.7; Ld = 0.8; Lq=0.254, a) stator currents, b) stator voltages, c) estimated rotor position.

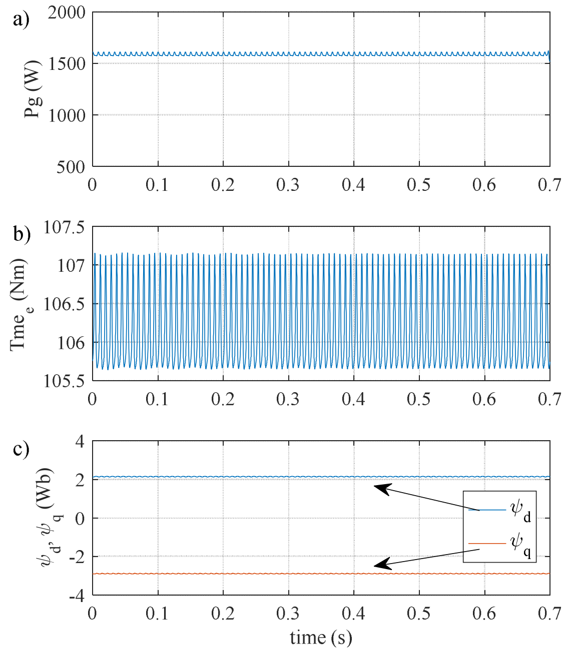

Fig. 7. High power results: i_d= 5; i_q= -10, Rs = 6.7; Ld = 0.8; Lq = 0.254, a) active output power, b) torque, c) dq flux linkages.

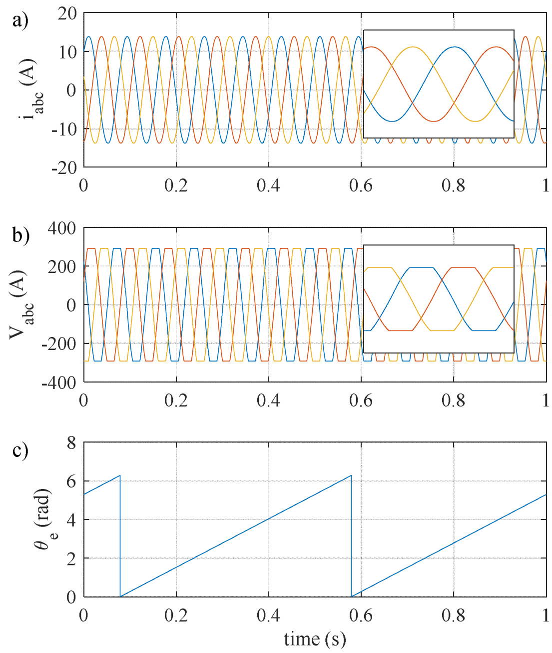

Fig. 8. Rated torque: i_d= 7.5; i_q = -15.5; Rs = 6.7; Ld = 0.555; Lq = 0.255, a) stator currents, b) stator voltages, c) estimated rotor position.

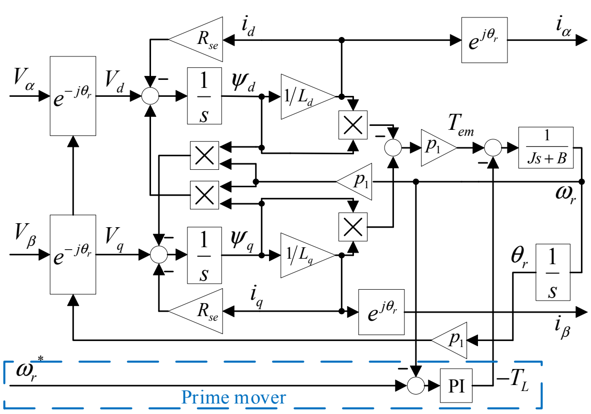

Fig. 9. SynRG with prime mover – block diagram

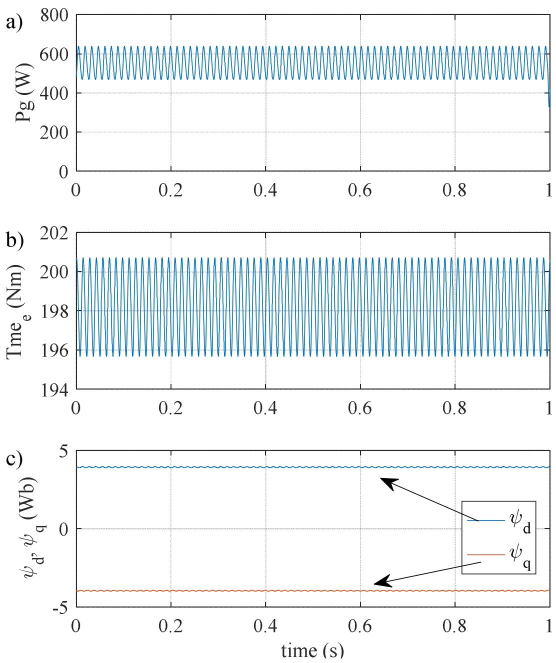

Fig. 10. Rated torque: i_d = 7.5; i_q = -15.5; *Rs* = 6.7; *Ld* = 0.555; *Lq* = 0.255, a) active output power, b) torque, c) dq flux linkages.

VI. EXPERIMENTAL RESULTS

The proposed control method was validated on a test bench as depicted in Fig. 11 and Fig. 12. The results for the corresponding setup are presented in Fig. 13 - Fig. 19. The SynRG has the parameters given in TABLE I. The SynRG is driven by a 11 kW three phase squirrel cage induction motor (IM), controlled by a back-to-back ABB (ACS 800) inverter. A 4 kVA Danfoss inverter feeds the SynRG. The control technique is implemented on a digital signal processor (dSpace DS1103). The Danfoss inverter control board was replaced with another interface card which provides full control over the inverter IGBT gate drivers.

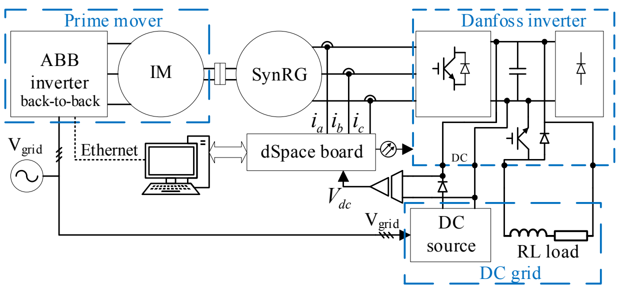

Fig. 11. Test setup diagram

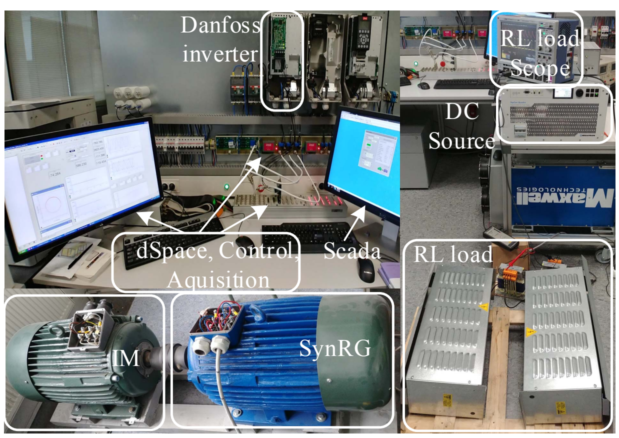

Fig. 12. Experimental platform

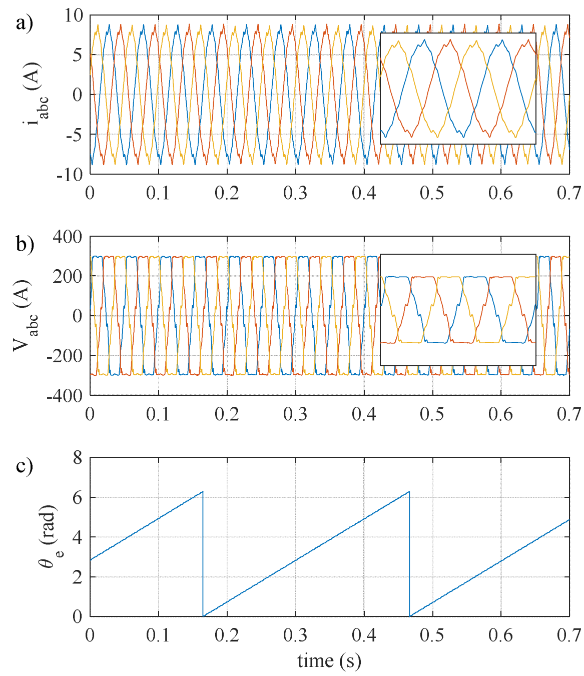

Fig. 13. Experimental results: $i_d^* = 5A$, $i_q^* = -10A$, $n = 200rpm$, a) stator currents, b) stator voltages, c) estimated rotor position.

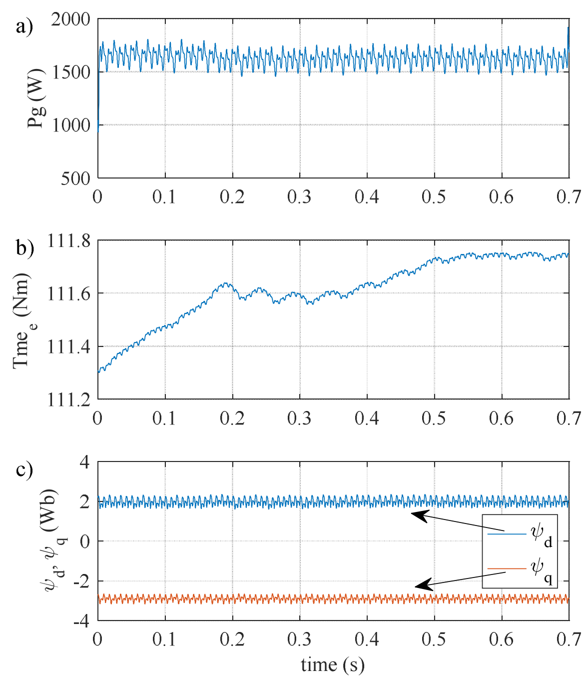

Fig. 14. Experimental results: $i_d^* = 5A$, $i_q^* = -10A$, $n = 200rpm$, a) active output power, b) torque, c) dq flux linkages.

The communication between dSpace and inverter is done through fiber optics for noise immunity and galvanic isolation. The phase currents and DC voltage are measured by the dSpace board. In order to emulate the DC grid, a DC source is used for keeping the voltage at 350V for inverter and measurement equipment feeding when the generator doesn't produce power. The load is represented by a chopper (inside the Danfoss inverter) with a RL load (*R*=60 Ω, *L*=9,36 mH). The chopper is controlled with a PI controller for maintaining the $V_{DC} = 580V$, implemented in dSpace. The reference DC voltage can be modified. The load voltage and current (V_{RL} , i_{RL}) are measured using an oscilloscope.

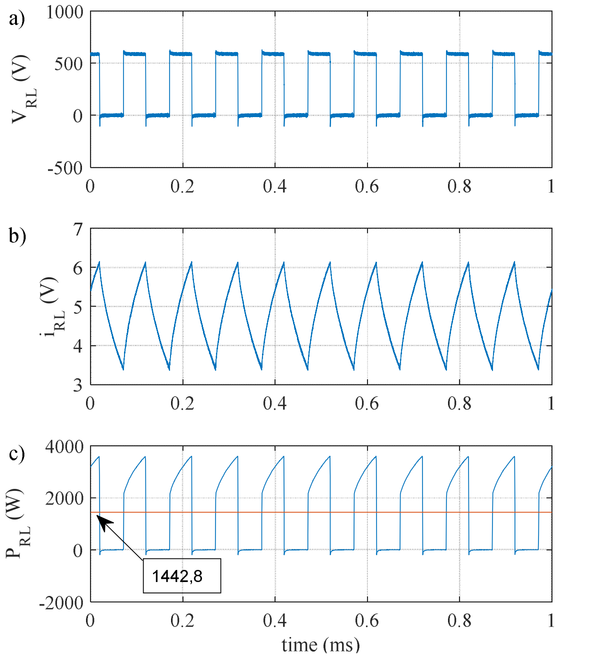

Fig. 15. Experimental results (RL load): $i_d^* = 5A$, $i_q^* = -10A$, $n = 200rpm$, a) load voltage, b) load current, c) load power.

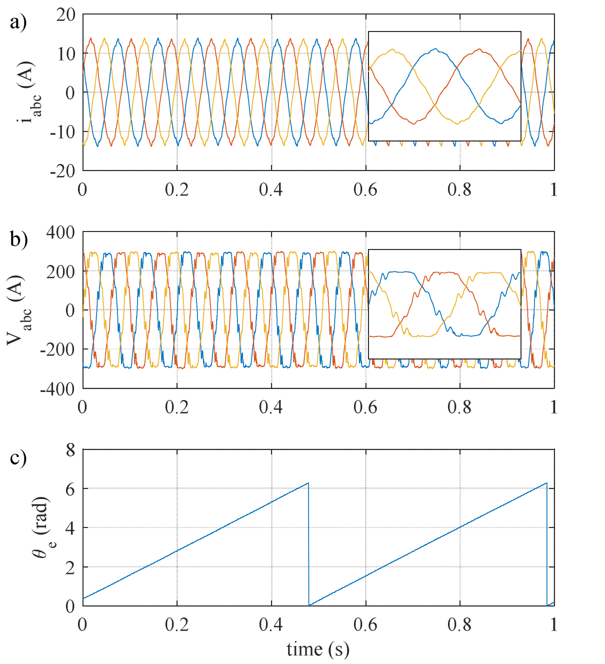

Fig. 16. Experimental results: $i_d^* = 7.5A$, $i_q^* = -15.5A$, $n = 120rpm$, a) stator currents, b) stator voltages, c) estimated rotor position..

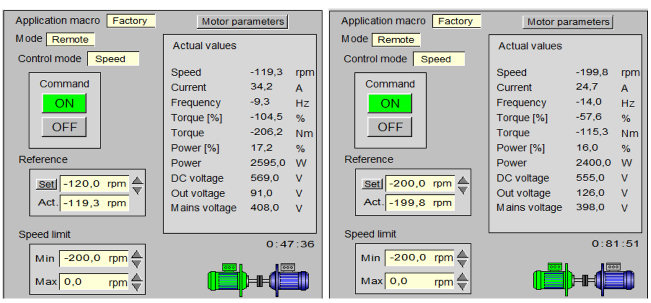

Fig. 17. SCADA actual values (left: $i_d^* = 5A$, $i_q^* = -10A$, $n = 200rpm$;right: $i_d^* = 7.5A$, $i_q^* = -15.5A$, $n = 120rpm$).

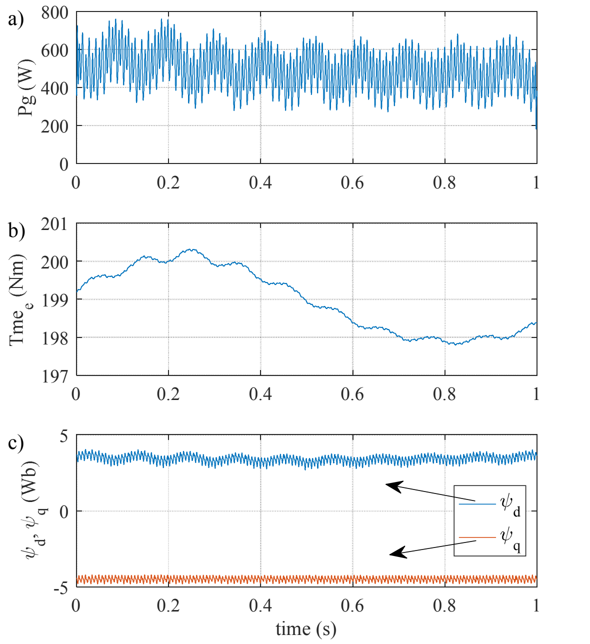

Fig. 18. Experimental results: $i_d^* = 7.5A$, $i_q^* = -15.5A$, $n = 120rpm$ a) active output power, b) torque, c) dq flux linkages.

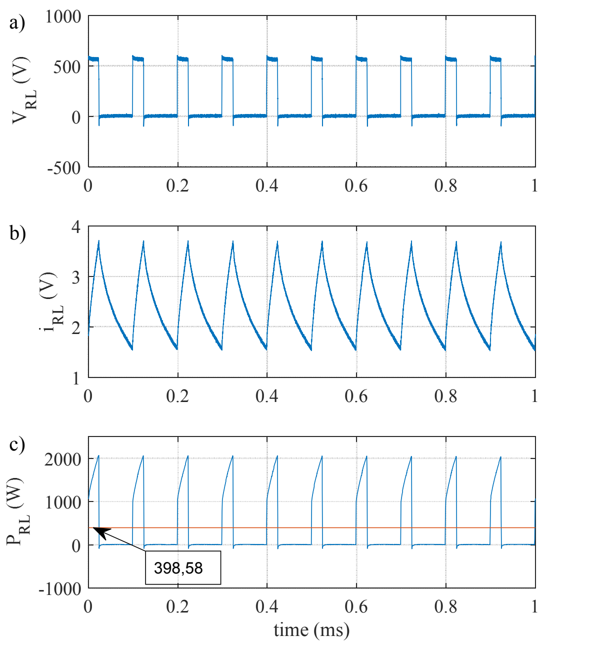

Fig. 19. Experimental results (RL load) $i_d^* = 7.5A$, $i_q^* = -15.5A$, $n = 120rpm$, a) load voltage, b) load current, c) load power.

Communication with ABB inverter is done through ethernet, protocol Modbus TCP/IP, using an adapter module (RETA-01). A SCADA system was developed (in Control Maestro software) for reference and actual values.

VII. Conclusions

Presented paper propose a different method for estimating the rotor position of a SynRG. The proposed method was successfully tested on a large speed respectively torque range, starting from 60 rpm up to 200 rpm respectively required torque for zero output power up to full load (around 200 Nm). The speed range covers requirements for wind and hydro generator applications. The experimental results show that torque and speed estimation by the proposed method are very close with the values given by the inverter of the driving machine Fig. 18. Lower speed in generator mode cannot be obtained due to the drop voltage on internal resistance of the machine. Extensive simulations and experimental results prove that the system is stable for the next ranges of the per unit estimator parameters: resistance variation between 0.71-1.35, d-axis inductance between 0.67-1.98, and q-axis inductance between 0.89- 1.18 from rated values.

This method could be an alternative for the existent sensorless control methods of the SynRG in order to avoid integrators offset, initial flux values compensation, and a DC voltage reserve (for the signal injection method).

The sensitivity and stability of position error method presented in this paper can be used also to analyze the performance of other rotor position estimators from literature (stator flux position angle [17], [21], [22] or active flux position angle [25]). The simulation and experimental results validated the proposed control method and with a larger Ld/Lq ratio (presented SynRG has only Ld/Lq=2.7 ratio), better energetical results can be obtained.

ACKNOWLEDGMENT

This work was supported by two grant of the Romanian Ministry of Research and Innovation, CCCDI – UEFISCDI, project number PN-III-P1-1.2-PCCDI-2017- 0391 / CIA_CLIM – *"Smart buildings adaptable to the climate change effects"*, within PNCDI III, and also, project number 10PFE/16.10.2018, PERFORM-TECH-UPT - *The increasing of the institutional performance of the Polytechnic University of Timișoara by strengthening the research, development and technological transfer capacity in the field of "Energy, Environment and Climate Change"*, Institutional Development Projects - Excellence Funding Projects in RDI, PNCDI III.

REFERENCES

[1] P. Roshanfekr, „Energy-efficient Generating System for HVDC Off-shore Wind Turbine", Chalmers University of Technology, Goteborg, Sweden, 2013.

[2] L. Castellini, M. D'Andrea, G. Fabri, D. Macera, şi M. Villani, „Design of a Synchronous Reluctance Machine for a Flywheel-Based Energy Storage System", în *2018 XIII International Conference on Electrical Machines (ICEM)*, 2018, pp. 2099–2104.

[3] „Reluctance Electric Machines: Design and Control", *CRC Press*. [Online]. Disponibil la: https://www.crcpress.com/Reluctance-Electric-Machines-Design-and-Control/Boldea-Tutelea/p/book/9781498782333. [Data accesării: 25-nov-2018].

[4] P. Roshanfekr, S. T. Lundmark, T. Thiringer, şi M. Alatalo, „Comparison of a 5MW permanent magnet assisted synchronous reluctance generator with an IPMSG for wind application", în *2014 International Conference on Electrical Machines (ICEM)*, 2014, pp. 711–715.

[5] P. Roshanfekr, S. Lundmark, T. Thiringer, şi M. Alatalo, „A synchronous reluctance generator for a wind application-compared with an interior mounted permanent magnet synchronous generator", în *7th IET International Conference on Power Electronics, Machines and Drives (PEMD 2014)*, 2014, pp. 1–5.

[6] R. H. Moncada, B. J. Pavez, J. A. Tapia, şi J. Pyrhönen, „Operation analysis of synchronous reluctance machine in electric power generation", în *2014 International Conference on Electrical Machines (ICEM)*, 2014, pp. 2734–2739.

[7] A. Vagati, G. Franceschini, I. Marongiu, şi G. P. Troglia, „Design criteria of high performance synchronous reluctance motors", în *Conference Record of the 1992 IEEE Industry Applications Society Annual Meeting*, 1992, pp. 66–73 vol.1.

[8] T. J. E. Miller, A. Hutton, C. Cossar, şi D. A. Staton, „Design of a synchronous reluctance motor drive", *IEEE Transactions on Industry Applications*, vol. 27, nr. 4, pp. 741–749, iul. 1991.

[9] T. Matsuo şi T. A. Lipo, „Rotor design optimization of synchronous reluctance machine", *IEEE Transactions on Energy Conversion*, vol. 9, nr. 2, pp. 359–365, iun. 1994.

[10] S. Guha şi N. C. Kar, „Saturation Modeling and Stability Analysis of Synchronous Reluctance Generator", *IEEE Transactions on Energy Conversion*, vol. 23, nr. 3, pp. 814–823, sep. 2008.

[11] S. Maroufian şi P. Pillay, „Self-excitation criteria of the synchronous reluctance generator in stand-alone mode of operation", în *2016 IEEE International Conference on Power Electronics, Drives and Energy Systems (PEDES)*, 2016, pp. 1–5.

[12] R. Sharma şi and B. Singh, „SyRG-PV-BES Based Standalone Microgrid Using Appoximate Multipliers Based Adaptive Control", în *2018 5th IEEE Uttar Pradesh Section International Conference on Electrical, Electronics and Computer Engineering (UPCON)*, 2018, pp. 1–6.

[13] R. H. Moncada, H. A. Young, B. J. Pavez-Lazo, şi J. A. Tapia, „A commercial-off-the-shelf synchronous reluctance motor as a generator for wind power applications", în *2015 IEEE International Electric Machines Drives Conference (IEMDC)*, 2015, pp. 6–12.

[14] J. C. Mitchell, M. J. Kamper, şi C. M. Hackl, „Small-scale reluctance synchronous generator variable speed wind turbine system with DC transmission linked inverters", în *2016 IEEE Energy Conversion Congress and Exposition (ECCE)*, 2016, pp. 1–8.

[15] S. Tokunaga şi K. Kesamaru, „FEM simulation of novel small wind turbine generation system with synchronous reluctance generator", în *2011 International Conference on Electrical Machines and Systems*, 2011, pp. 1–6.

[16] M. Alnajjar şi D. Gerling, „Medium-Speed Synchronous Reluctance Generator as Efficient, Reliabile and Low-Cost Solution for Power Generation in Modern Wind Turbines", în *2018 International Symposium on Power Electronics, Electrical Drives, Automation and Motion (SPEEDAM)*, 2018, pp. 1233–1238.

[17] D. V. M, B. Singh, şi B. G, „Position Sensor-less Synchronous Reluctance Generator Based Grid-Tied Wind Energy Conversion System with Adaptive Observer Control", *IEEE Transactions on Sustainable Energy*, pp. 1–1, 2019.

[18] T. Mabuchi *et al.*, „Position sensorless control of synchronous reluctance motors at very low speeds region using high-frequency current control system", în *2017 20th International Conference on Electrical Machines and Systems (ICEMS)*, 2017, pp. 1–6.

[19] I. Boldea, Z. Fu, şi S. A. Nasar, „Sensorless DC output control of a high performance reluctance generator system", în *Proceedings of 1994 IEEE Industry Applications Society Annual Meeting*, 1994, vol. 1, pp. 16–22 vol.1.

[20] I. Boldea şi S. C. Agarlita, „The active flux concept for motion-sensorless unified AC drives: A review", în *International Aegean Conference on Electrical Machines and Power Electronics and Electromotion, Joint Conference*, 2011, pp. 1–16.

[21] X. Dianguo, J. Xinhai, şi C. Wei, „Sensorless control of synchronous reluctance motors", în *2017 IEEE Transportation Electrification Conference and Expo, Asia-Pacific (ITEC Asia-Pacific)*, 2017, pp. 1–4.

[22] I. BOLDEA, Z. X. FU, şi S. A. NASAR, „Torque Vector Control (tvc) of Axially-Laminated Anisotropic (ala) Rotor Reluctance Synchronous Motors", *Electric Machines & Power Systems*, vol. 19, nr. 4, pp. 533–554, iul. 1991.

[23] S. Agarlita, I. Boldea, şi F. Blaabjerg, „High-Frequency-Injection-Assisted "Active-Flux"-Based Sensorless Vector Control of Reluctance Synchronous Motors, With Experiments From Zero Speed", *IEEE Transactions on Industry Applications*, vol. 48, nr. 6, pp. 1931–1939, nov. 2012.

[24] I. Boldea, M. C. Paicu, şi G. Andreescu, „Active Flux Concept for Motion-Sensorless Unified AC Drives", *IEEE Transactions on Power Electronics*, vol. 23, nr. 5, pp. 2612–2618, sep. 2008.

[25] S. Agarliţă, M. Fătu, L. N. Tutelea, F. Blaabjerg, şi I. Boldea, „I-f starting and active flux based sensorless vector control of reluctance synchronous motors, with experiments", în *2010 12th International Conference on Optimization of Electrical and Electronic Equipment*, 2010, pp. 337–342.